

Non-monotonic Irreversibility in Polytropic Steering

Cong Fu^{1,2}, Youhui Lin², Shanhe Su^{2*}, Yu-Han Ma^{1,3*}

¹School of Physics and Astronomy, Beijing Normal University, Beijing, 100875, China.

²Department of Physics, Xiamen University, Xiamen, 361005, Fujian, China.

³Key Laboratory of Multiscale Spin Physics (Ministry of Education), Beijing Normal University, Beijing, 100875, China.

*Corresponding author(s). E-mail(s): sushanhe@xmu.edu.cn; yhma@bnu.edu.cn;

Contributing authors: fucong@stu.xmu.edu.cn; linyouhui@xmu.edu.cn;

Abstract

The efficient manipulation of thermodynamic states within the finite time is fundamentally constrained by the intrinsic dissipative cost. While the slow-driving regime is well-characterized by a universal $1/\tau$ -scaling of irreversibility, the physics governing fast, non-adiabatic transitions remains elusive. Here, we propose the polytropic steering protocols that provide an exact analytical bridge between the isothermal and adiabatic limits for Brownian particles far-from-equilibrium. We demonstrate that for any protocol duration τ , the system can be precisely steered along a prescribed polytropic trajectory, revealing a striking non-monotonic dependence of irreversibility on the driving rate. Contrary to the near-equilibrium paradigm where faster driving necessitates higher energetic costs, we identify a *most-irreversible* timescale, beyond which dissipation is anomalously suppressed by rapid driving. By mapping these protocols onto a broad class of controllable thermodynamic cycle, we establish power-efficiency tradeoffs and position the polytropic index as a genuine thermodynamic control knob for the rational design of high-speed, high-performance microscopic thermal machines.

Introduction

The ability to steer thermodynamic transformations is fundamental to the development of energy conversion technologies, spanning from classical heat engines to emerging quantum devices [1–4]. Since Sadi Carnot [5], the conceptual bedrock of thermodynamics has rested on the Carnot cycle, a reversible sequence formed by linking isothermal processes in quasi-static thermal equilibrium with adiabatic processes in perfect heat isolation. These idealized processes culminate in the Carnot efficiency, which set a fundamental upper bound for all thermodynamic cycles. Yet, when downsizing to the mesoscopic scale, where thermal fluctuations dominate and operational speed becomes

critical, these textbook paradigms face profound challenges [6–10]. A fundamental question thus arises: can we construct a thermodynamic bridge that transcends the rigid isothermal-adiabatic dichotomy, offering a continuum of processes tunable in both reversibility and speed?

Recent advances in stochastic thermodynamics have revealed the inevitable energetic cost of finite-time operations, establishing that irreversible entropy generation (IEG) typically diverges as $1/\tau$ in slow-driving (near-equilibrium) processes of duration τ [11–16]. This universal scaling underpins the conventional perception that faster driving necessitates higher dissipation. Yet, this *faster-requires-more* paradigm is largely a hallmark of the linear-response regime [1, 15, 17],

[18]. Far from equilibrium, the complex interplay between driving protocols and thermal relaxation unlocks remarkably richer, non-linear dissipative behaviors [15, 19–26], where the traditional constraints on irreversibility might be circumvented.

Here, we introduce the finite-time polytropic process for Brownian particles. By defining a time-dependent polytropic index $\xi(\tau)$, we establish an exact analytical bridge that continuously interpolates between the isothermal and adiabatic limits. We derive the rigorous control protocols required to steer the system along prescribed polytropic trajectories at arbitrary speeds. Remarkably, our results uncover a striking non-monotonic dependence of irreversibility on τ : the IEG reaches a maximum at intermediate timescales and vanishes at both the quench and quasi-static limit. Our framework provides full analytical control over the partitioning of energy into work and heat, enabling the design of microscale thermodynamic cycles with tunable power-efficiency characteristics. By replacing the rigid isothermal-adiabatic binary with a continuous spectrum of polytropic processes, this work offers a versatile tool for the rational design of high-speed, high-efficiency energy converters at the micro-scale.

Results

Polytropic steering of Brownian particles

We consider a underdamped Brownian particle of mass m confined in a time-dependent potential $U(x, k_t) = k_t x^{2n}/(2n)$ with k_t the stiffness. The particle is coupled to a heat reservoir at temperature T_s and experiences viscous damping with coefficient γ . The motion of the particle is governed by the complete Langevin equation [27]

$$\ddot{x} + \gamma \dot{x} + \frac{k_t}{m} x^{2n-1} = \frac{\zeta(t)}{m}, \quad (1)$$

where $x(t)$ denotes the particle position and the stochastic force $\zeta(t)$ is the white noise. In the underdamped regime where $\sqrt{k_t/m} \gg \gamma$, such stochastic dynamics leads to a master equation for the particle energy $E(x, p) = m\dot{x}^2/2 + U(x, k_t)$. Using Ito's lemma and the virial theorem, the

stochastic energy conservation relation reads [28]

$$dE = \frac{\dot{\lambda}}{\lambda} E dt - \Gamma_n (E - \frac{f_n T_s}{2}) dt + \sqrt{2\Gamma_n T_s E} dW_t, \quad (2)$$

where $\lambda(t) \equiv k_t^{2/(n+1)}$ is the work parameter, $\Gamma_n \equiv 2n\gamma/(n+1)$ is the effective friction coefficient, and $f_n \equiv (n+1)/n$. Here, dW_t denotes the increment of a Wiener process (the full derivations are detailed in Section 1 of the Supplemental Materials). To achieve the controlled evolution of the system, we propose the finite-time polytropic process of a Brownian particle defined by the following invariant relation

$$\theta(t)\lambda^\xi(t) = \text{const}, \quad \xi \in \mathbb{R}, \quad (3)$$

with $\theta(t) \equiv 2 \langle E(t) \rangle / f_n$ the instantaneous effective temperature of the particle, and $t \in [0, \tau]$. Note that the separated timescales $\tau_{\text{in}} \ll \tau, \tau_{\text{r}}$ underpin the above finite-time control task, where $\tau_{\text{in}} \sim \sqrt{nm/k_t}$ is the trap oscillation period, and $\tau_{\text{r}} = \Gamma_n^{-1}$ is the thermalization time. This separation ensures that the system completes many oscillations within the driving timescale, allowing the particle to establish, at any instant, an approximate local equilibrium distribution. Hereafter, unlike the common assumption of slow-driving with $\tau \gg \tau_{\text{r}}$ [14, 15, 18, 27], we impose no restrictions on the relative sizes of τ and τ_{r} . Therefore, both near-equilibrium slow-driving and far-from-equilibrium fast-driving ($\tau \ll \tau_{\text{r}}$) regimes are covered. These two regimes are associated with the isothermal ($\xi = 0$) and adiabatic ($\xi = -1$) limits, respectively. The polytropic construction selects a structured subclass of trajectories in the (λ, θ) control space, continuously interpolating between two limiting processes. In doing so, it captures the essential features of a much broader family of nonequilibrium drivings and serves as a reduced representation of energetics in the full protocol space. Imposing Eq. (3) reduces the coupled stochastic dynamics in Eq. (2) to a single, time evolution with respect to $\theta(t)$. For $\theta|_{t=0} \equiv \theta_0 = (1 + \delta) T_s$ with δ measures the initial temperature offset from the reservoir, the finite-time control protocol is solved as

$$\lambda(t) = \lambda_0 \left[\frac{\delta}{1 + \delta} \exp \left(-\frac{\xi \Gamma_n}{\xi + 1} t \right) + \frac{1}{1 + \delta} \right]^{-\frac{1}{\xi}} \quad (4)$$

with $\lambda(0) \equiv \lambda_0$. Equation (4) therefore provides an exact, experimentally implementable family of finite-time polytropic protocols, hereafter referred to as *polytropic steering*.

Traditionally, polytropic processes are treated as a sequence of quasi-static equilibrium states, collapsing the temporal dimension. Polytropic steering extends this conventional framework by explicitly incorporating the time dimension, as illustrated in the spatiotemporal diagram [Fig. 1(a)]. Our approach reveals that the finite-time path is uniquely determined by the coupling between the prescribed energy evolution [Eq. (2)] and the underlying geometric constraints [Eq. (3)] of the parametric space. It is worth noting that polytropic steering requires nonequilibrium initial states; otherwise, only isochoric (constant stiffness) or isothermal processes are possible. This constraint reflects the necessity of initial heat flow in quasi-static protocols. The process trajectory is externally constrained, balancing work against heat exchange. Equation (4) further show that the initial effective temperature relative to the reservoir controls the process direction: $\delta < 0$ for expansion ($\lambda \downarrow$), while $\delta > 0$ for compression ($\lambda \uparrow$). A detailed analysis of the singularity at $\delta = 0$ and the global dependence of δ is provided in Section 4 of the Supplemental Materials. Particularly, for the quasi-isothermal process of $\xi = 0$, Eq. (4) reduces to $\lambda(t) = \lambda_0 (\lambda_f/\lambda_0)^{t/\tilde{\tau}}$ with $\lambda(\tau) \equiv \lambda_f$, which recovers the result of Ref. [10]. The key to achieving polytropic steering with different ξ is to change the control duration of the process. It follows from Eq. (4) that

$$\tilde{\tau} = -(1 + \xi^{-1}) \ln [(1 + \delta^{-1})u^{-\xi} - \delta^{-1}], \quad (5)$$

where $u \equiv \lambda_f/\lambda_0$ and $\tilde{\tau} \equiv \tau/\tau_r$. As shown in Fig. 1(b), achieving ξ from 0 (isothermal) to -1 (adiabatic) requires tuning driving speed from slow to fast.

A defining feature of the proposed polytropic steering paradigm is its fundamental independence from the specific damping regime. While the analytical framework is initially developed for the underdamped case, it extends naturally to the overdamped regime, which is of particular significance for experimental realizations in colloidal setups [29] and biological micro-environments [30]. In this regime, the polytropic constraint translates from an explicit protocol into a differential

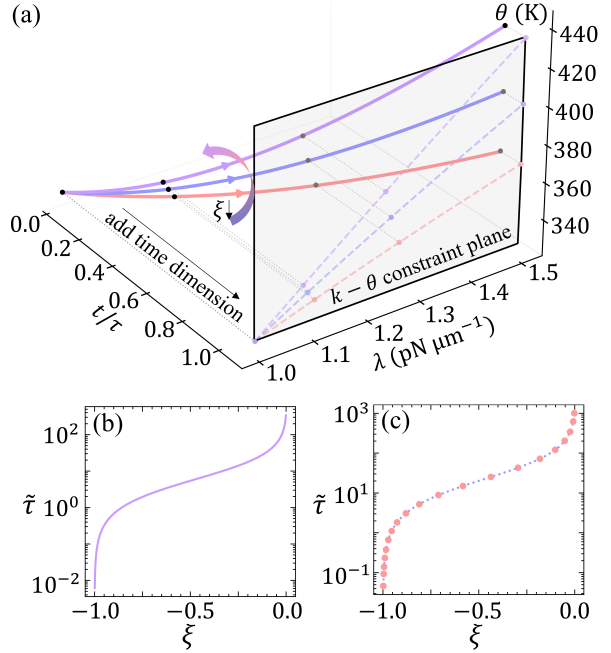


Fig. 1 (a) The finite-time evolution of the thermodynamic state (λ, θ) as a function of normalized time t/τ for polytropic index $\xi = -0.3$ (red), $\xi = -0.5$ (blue), and $\xi = -0.7$ (purple). The dashed curves projected on the shaded gray plane are given by the polytropic constraint $\theta\lambda^\xi = \text{const}$. The dimensionless process duration $\tilde{\tau}$ as a function of ξ for underdamped regime (b) and overdamped regime (c), where simulation data are represented by pink dots. In this figure, $u = 1.5$ and $\delta = 1 \times 10^{-3}$ are used.

steering equation. For instance, for overdamped Brownian particles trapped in a harmonic potential ($n = 1$), the control protocol is governed by

$$\frac{\dot{k}_t}{k_t} = \frac{2k_t}{m\gamma(\xi + 1)} \left[1 - \frac{1}{1 + \delta} \left(\frac{k_t}{k_0} \right)^\xi \right], \quad (6)$$

which reflects the intrinsic coupling between the effective heat transfer and the control parameter. Despite the implicit nature of this protocol, the resulting τ - ξ maintains a trend consistent with the underdamped case, as validated by our numerical solutions of the full Langevin dynamics, which is illustrated in Fig. 1(c). The simulation data (pink dots) validate the theoretical result (blue dotted curve) of Eq. (6). Derivation details are provided in Section 2 of the Supplemental Materials. This extension underscores the operational versatility

of our framework across diverse experimental platforms, providing an analytically tractable bridge between different dynamical regimes. As a concrete and novel illustration of the overdamped design, for $\xi = 0$, Eq. (6) yields $k_t^{-1} = k_0^{-1} - 2\delta t/[m\gamma(1 + \delta)]$, which furnishes an analytically tractable protocol realizing the endoreversible isothermal stroke.

Irreversibility and energetics of polytropic steering

Irreversibility, a fundamental manifestation of the second law of thermodynamics, serves as an essential concept for understanding non-equilibrium phenomena across diverse systems [31]. On a quantitative level, IEG was proposed to quantify the deviation between equilibrium and non-equilibrium thermodynamic processes [32], widely employed in physics, chemistry, and biology [1, 33, 34]. For practical applications, engineering IEG is crucial for designing energy-efficient technologies from micro to macro scales [34–37]. The quantification of irreversibility has been widely studied [38, 39]. In the near-equilibrium regime, specifically when the process duration $\tau \gg \tau_r$, IEG follows as Σ/τ [11–15, 18, 40]. This $1/\tau$ -scaling, with the coefficient Σ dictated by the specific driving protocol [15, 16, 41], is crucial for designing efficient heat engines [14, 18], minimizing the energy cost of information erasure [42], and optimizing particle separation [43]. Recent experimental [15] and numerical [19] findings show that IEG in the fast-driving regimes significantly departs from the typical $1/\tau$ -scaling. As the driving time increases, the change of IEG as it varies across the short- to long-time regime has not yet been revealed. In the following, we reconcile the IEG behaviors across different time regimes using the framework of finite-time polytropic processes. For these processes, the IEG is analytically derived as

$$\Delta S_{\text{ir}} = \chi(\xi+1) [\xi^{-1}(1 + \delta)(1 - u^{-\xi}) - \ln u], \quad (7)$$

where $\chi \equiv \langle E \rangle/\theta(t) = f_n/2$ for underdamped Brownian particles; while $\chi = 1/2$ for overdamped particles trapped in a harmonic potential.

The dependence of the IEG on the protocol duration $\tilde{\tau}$ is depicted in Fig. 2(a), obtained by combining Eq. (7) with Eq. (5). The profile

reveals two distinct asymptotic regimes: in the fast-driving limit ($\tilde{\tau} \ll 1$), the IEG grows linearly with time, $\Delta S_{\text{ir}} \sim \kappa_1(\delta, u)\tilde{\tau}$; conversely, in the quasi-static limit ($\tilde{\tau} \gg 1$), the system recovers the universal $1/\tilde{\tau}$ -scaling, $\Delta S_{\text{ir}} \sim \kappa_2(\delta, u)/\tilde{\tau}$ ($\kappa_{1,2}(\delta, u)$ are provided in the Supplemental Materials, Section 3). Crucially, Eq. (7) predicts a non-monotonic dependence in the intermediate regime, reaching a local maximum ($\Delta S_{\text{ir}}^{(\text{max})}$) marked by the purple triangle in Fig. 2(a)) that defines a 'most-irreversible' protocol. This behavior, which echoes observations in quantum thermodynamic systems [44], arises from a competition between the instantaneous dissipation rate and the process duration: while shorter durations intensify transient heat fluxes due to larger temperature gradients, the total entropy production is eventually constrained by the vanishing time available for heat exchange. The interplay between these two effects results in a peak of irreversibility at a characteristic timescale.

To verify the robustness of the non-monotonicity and the controllability of the IEG, we examine how the system configuration, specifically the initial temperature offset δ and the compression ratio u , modulates the dissipation profiles in Figs. 2(b) and (c). Physically, δ quantifies the initial thermodynamic drive and a larger δ pushes the system further from equilibrium, inducing a more intense initial heat flow $J = -\gamma\delta T_s$. This strengthens the transient heat exchange and consequently elevates the irreversible cost across all accessible timescales. Meanwhile, the compression ratio u dictates the extent of the trajectory in parametric space. As u increases, the system undergoes a broader thermodynamic transformation, naturally scaling up the total dissipation as the particle traverses a 'longer' path under the same steering constraints. A distinctive feature in these profiles is the emergence of a maximum protocol duration $\tilde{\tau}_{\text{max}}$ (indicated by markers) in the endoreversible limit ($\xi \rightarrow 0$). This $\tilde{\tau}_{\text{max}}$ represents a fundamental compatibility limit: beyond this threshold, the prescribed heat exchange with the reservoir can no longer be balanced by the control work required to maintain the polytropic invariant. This marks a regime where the reservoir's thermal relaxation capacity becomes insufficient to support the steering protocol (see Section 4 of the

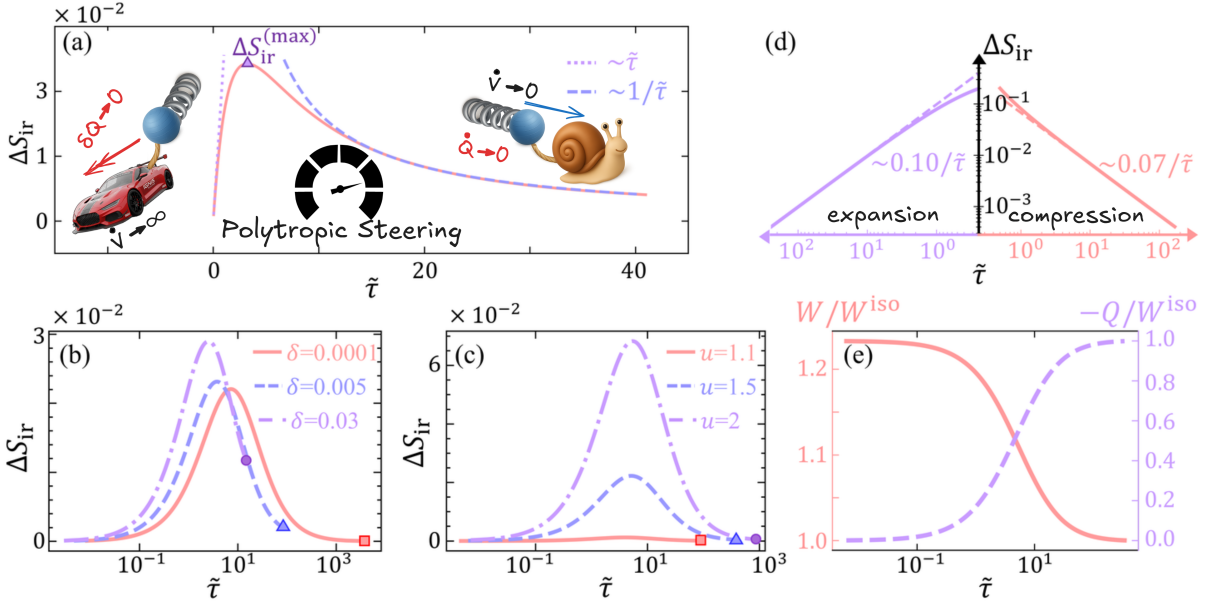


Fig. 2 (a) IEG ΔS_{ir} as a function of the dimensionless process duration $\tilde{\tau}$ (solid red curve). ΔS_{ir} versus $\tilde{\tau}$ for different δ (b) and u (c). In these two plots, the maximum process durations $\tilde{\tau}_{max}$ associated with $\xi = 0$ are marked with different markers. (d) ΔS_{ir} as a function of the process duration τ for endoreversible isothermal processes (solid curve, $\xi = 0$). The left (right) axis is associated with $u = 3/2$ ($u = 2/3$). The dashed line represent the predicted asymptotic scaling. (e) Normalized work W (pink solid curve) and heat $-Q$ (purple dashed curve) as a function of process duration, where $W_{iso} = \theta_0 \ln u$. To plot (a) and (e), we set $u = 1.5$ and $\delta = 1 \times 10^{-2}$.

Supplemental Materials for details). While the parametric studies in Figs. 2(b) and (c) illustrate the global scaling of irreversibility, they also hint at a deeper dependence on the direction of the process. To unveil this, we focus on the scenario of $\xi \rightarrow 0$ to examine the potential symmetry breaking between expansion and compression Fig. 2(d), where the left and right panels correspond to expansion ($u = 3/2$) and compression ($u = 2/3$) protocols, respectively. In the long-time regime, both processes follow a $1/\tau$ -scaling; however, in the short-time regime, the IEG for compression exceeds the scaling law, whereas the IEG for expansion falls below it. Furthermore, the global dependence on δ , which characterizes the transition from endoreversible to fully reversible isothermal processes, is provided in Section 4 of the Supplemental Materials.

We then shift our focus from the irreversibility to energetics of the polytropic steering to elucidate how work and heat are partitioned far from equilibrium. The polytropic index ξ acts as a control knob, interpolating between the isothermal ($\xi =$

0) and adiabatic ($\xi = -1$) limits [45]. Unlike conventional near-equilibrium frameworks that rely on perturbative expansions, our approach yields exact analytical expressions for work and heat valid for arbitrary protocol durations. Starting from the ensemble-level first law of thermodynamics, $d\langle E \rangle = dW + dQ$, with $\langle E \rangle = \chi\theta(t)$, we find the total work input $W = \chi\xi^{-1}T_s(1+\delta)(1-u^{-\xi})$ and the absorbed heat $Q = -(1+\xi)W$. The linear relation, $Q \propto W$, reveals that the polytropic constraint enforces a rigid energy-partitioning rule regardless of the driving speed. As illustrated in Fig. 2(e), varying the duration $\tilde{\tau}$ provides quantitative control over the magnitude of energy transfer. The isothermal ($\xi = 0$) and adiabatic ($\xi = -1$) cases emerge as special points where the injected work is either entirely dissipated as heat ($Q + W = 0$, $\Delta E = 0$) or entirely stored/released as internal energy ($Q = 0$), respectively. This unified description highlights how finite-time driving can simultaneously modulate energy redistribution and the accompanying thermodynamic cost.

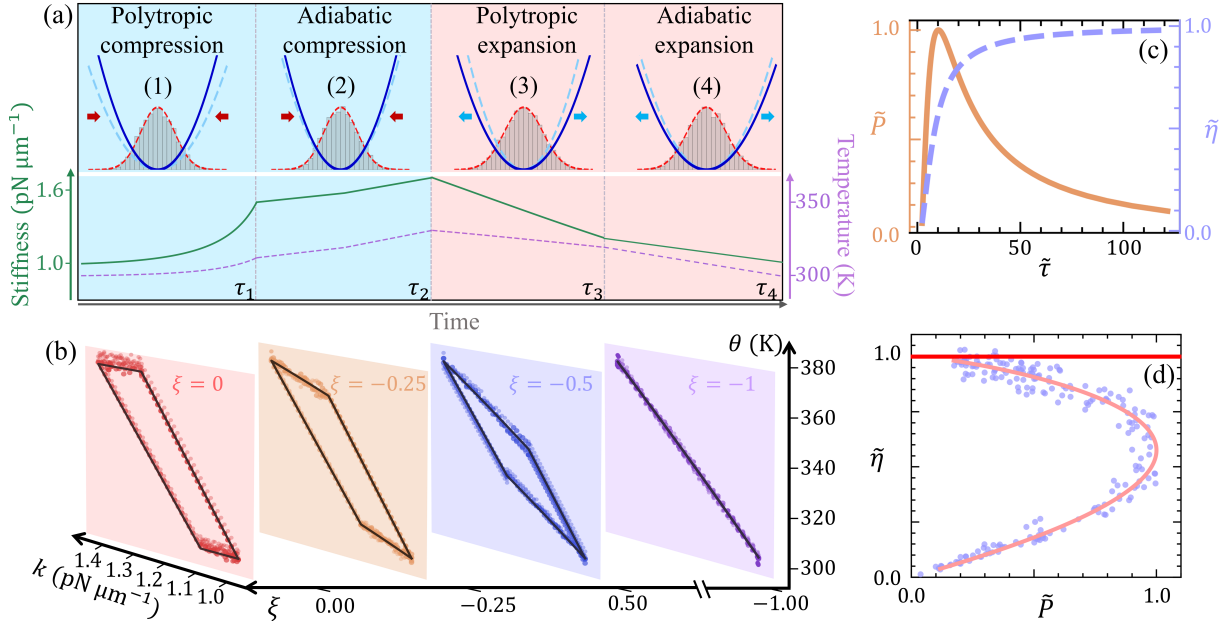


Fig. 3 The Brownian polytropic engine. (a) The time evolution of the polytropic protocol. (b) Thermodynamic diagrams for the transition of $\xi = -1, -0.5, -0.25$, and 0 . (c) Normalized power $\tilde{P} \equiv P/P_{\max}$ (orange solid curve), and efficiency $\tilde{\eta} \equiv \eta/\eta_C$ (blue dashed curve), versus $\tilde{\tau}$. (d) The power–efficiency trade-off (pink solid curve). The Simulation data are shown as blue dots and the red line indicates the Carnot efficiency.

Brownian polytropic cycles

The experimental realization of arbitrary thermodynamic cycles for Brownian particles is a formidable challenge, primarily due to the technical difficulty of simultaneously modulating the confinement potential and the particle’s effective temperature along a prescribed path [9]. The current proposed polytropic steering framework resolves this by providing a unified, precisely controllable protocol that spans a broad class of thermodynamic processes. To demonstrate its versatility, we construct a generic four-stroke heat engine cycle consisting of two polytropic strokes ($\xi \in [-1, 0]$) interleaved by two rapid adiabatic transitions ($\xi = -1$). As shown in the upper panel of Fig. 3(a), the probability distributions obtained from Langevin simulations (gray histograms) perfectly match our theoretical predictions (red dashed lines), validating the stability of the steering under thermal fluctuations (simulation details are provided in Section 5 of the Supplemental Materials). The cycle operates as follows: (i) polytropic compression while rejecting heat to a cold reservoir (T_c); (ii) adiabatic compression; (iii) polytropic expansion while

absorbing heat from a hot reservoir (T_h); and (iv) adiabatic expansion back to the initial state. Crucially, as exemplified for the case of $\xi = -0.2$ in Fig. 3(a) (lower panel), the time-dependent trap stiffness k_t and the effective temperature θ are co-modulated in a deterministic manner, ensuring the system strictly adheres to the polytropic invariant throughout the finite-time operation.

By integrating the overdamped Langevin dynamics with our derived protocols, we characterize the engine’s performance across the full parametric range. Fig. 3(b) maps these cycles in the $k - \theta$ (stiffness-temperature) state space. The remarkable agreement between simulation (markers) and theory (solid lines) underscores the robustness of the framework. We observe a clear geometric transition: at $\xi = 0$, the cycle operates as an endoreversible Carnot-like cycle; as ξ decreases toward -1 , the cycle area, representing the net work performed per cycle, gradually contracts, eventually collapsing into a single adiabatic curve where the work-heat exchange vanishes. Here, ξ emerges as a thermodynamic control knob that not only dictates the protocol shape but also governs the energy partitioning between work

and heat of the cycles, offering an unprecedented degree of control over the engine's output. The performance of heat engines is quantified by the efficiency $\eta = -W_{\text{net}}/Q_{\text{in}}$ and average output power $P = -W_{\text{net}}/\tau_{\text{cyc}}$. Here, $W_{\text{net}} = \sum W_i$ ($i = 1, 2, 3, 4$), while the heat input Q_{in} is defined by the energy absorbed from the hot reservoir, and $\tau_{\text{cyc}} = \sum \tau_i$ is the total cycle duration.

The practical power of this framework lies in its ability to map the complete power-efficiency landscape of microscopic engines. In Fig. 3(c), the normalized power \tilde{P} and efficiency $\tilde{\eta}$ reveal the intrinsic constraints imposed by finite-time driving. Notably, while \tilde{P} exhibits a non-monotonic dependence on $\tilde{\tau}$, reflecting the classic competition between driving frequency and dissipative loss, the efficiency $\tilde{\eta}$ approaches the Carnot limit monotonically. This disparity reveals a subtle thermodynamic competition: in the fast driving regime ($\tilde{\tau} \rightarrow 0$), although the absolute irreversible entropy generation ΔS_{ir} might be suppressed (as discussed in Fig. 2), the heat absorbed from the hot reservoir Q_{in} vanishes even more rapidly due to the geometric collapse of the cycle. This leads to a divergent relative cost of irreversibility, effectively suppressing efficiency at high speeds. Finally, Fig. 3(d) illustrates the distinct power-efficiency trade-off curve generated by varying ξ via τ . The theoretical result (light red curve) exhibits good agreement with the simulation data points. This cycle performance landscape provides a systematic route for identifying the optimal operating regime, spanning from the high-efficiency isothermal limit to the power-optimized regimes of finite-time polytropic processes, thus offering a blueprint for the design of high-performance microscopic heat engines.

Discussions

Our findings challenge the conventional perception *faster requires more consumption* for finite-time processes in non-equilibrium thermodynamics. By introducing the finite-time polytropic steering, we demonstrate that irreversibility is not an inevitable monotonic penalty for faster driving. Instead, the emergence of a 'most-irreversible' timescale signifies a unique dissipative peak, beyond which rapid driving actually suppresses entropy generation, a striking departure from the universal $1/\tau$ -scaling hold in the near-equilibrium

regime. This discovery bridges the gap between fundamental dissipation limits and the operational performance of finite-time heat engines. Beyond its theoretical elegance, the polytropic index ξ emerges as a genuine thermodynamic control knob, enabling the precision engineering of thermodynamic trajectories. By co-modulating control parameters along prescribed polytropic paths, this paradigm allows experimentalists to navigate and optimize the complex power-efficiency landscape. The validity of this framework transcends specific stochastic systems and because it is rooted in the fundamental evolution of energy, it scales seamlessly from the fluctuation-dominated realm of biological molecular motors to the macroscopic dynamics of gas turbines. We provide a systematic study on the finite-time polytropic steering of ideal gas in Section 6 of the Supplemental Materials. This extensibility is of profound significance for engineering applications, as most real-world thermal machines, such as internal combustion engines and gas turbines, operate along polytropic-like pathways where heat exchange and work extraction are coupled in finite time [46].

Looking forward, the polytropic steering paradigm opens several tantalizing avenues for exploration. First, the extension of this framework into the quantum regime promises to unveil how quantum coherence and entanglement modulate the non-monotonic dissipation landscape, potentially offering a quantum speedup for thermodynamic control [24]. Second, in the realm of active matter, where systems are driven by non-conservative internal forces, our steering protocol could provide a systematic route to harness energy from active baths, redefining the boundaries of work extraction in non-reciprocal environments [47]. Finally, by integrating our approach with information thermodynamics, one could explore the finite-time costs of information erasure and feedback control, potentially pushing the limits of high-speed, low-dissipation information processing and computing [42]. By replacing the traditional, rigid isothermal-adiabatic binary with a continuous spectrum of tunable processes, our work establishes a versatile blueprint for the next generation of high-speed, high-efficiency energy converters from the sub-atomic to the industrial scale.

Supplementary information. The Supplementary Information accompanying this paper provides extended theoretical derivations and technical details. It includes: (1) the detailed derivation for polytropic steering of underdamped Brownian particles; (2) the rigorous stochastic derivation for polytropic steering of overdamped Brownian particles; (3) the analytical asymptotic scaling laws for irreversible entropy generation; (4) a comprehensive analysis of the role of the initial temperature offset δ in determining process feasibility and dissipation; (5) the technical descriptions of the numerical solution for the control protocols, Langevin dynamics simulation methods, and verification of convergence and robustness; and (6) the systematic study on polytropic steering of macroscopic ideal gas systems.

Acknowledgements. We thank J.-C.C. for helpful comments. Y.-H.M. thanks the National Natural Science Foundation of China for support under grant No. 12305037 and the Fundamental Research Funds for the Central Universities under grant No. 2023NTST017. S.H.S thanks the National Natural Science Foundation of China for support under Grant No. 12364008, the Natural Science Foundation of Fujian Province for support under Grant No.2023J01006, and the Fundamental Research Fund for the Central Universities of China for support under Grant No.20720240145.

Author contributions. C.F. performed the theoretical study and numerical simulations. Y.H.L. supported the simulation aspects. S.H.S. supported the theoretical and simulation aspects and supervised the project. Y.-H.M. proposed, established, supervised the project, and developed its foundational theoretical framework. All authors discussed the results and wrote the manuscript.

References

- [1] M. Esposito, U. Harbola, S. Mukamel, Nonequilibrium fluctuations, fluctuation theorems, and counting statistics in quantum systems. *Rev. Mod. Phys.* **81**(4), 1665–1702 (2009). <https://doi.org/10.1103/RevModPhys.81.1665>
- [2] M. Campisi, P. Hänggi, P. Talkner, *Colloquium* : Quantum fluctuation relations: Foundations and applications. *Rev. Mod. Phys.* **83**(3), 771–791 (2011). <https://doi.org/10.1103/RevModPhys.83.771>
- [3] J.P. Pekola, Towards quantum thermodynamics in electronic circuits. *Nat. Phys.* **11**(2), 118–123 (2015). <https://doi.org/10.1038/nphys3169>
- [4] S. Vinjanampathy, J. Anders, Quantum thermodynamics. *Contemp. Phys.* **57**(4), 545–579 (2016). <https://doi.org/10.1080/00107514.2016.1201896>
- [5] S. Carnot, Réflexions sur la puissance motrice du feu et sur les machines propres à développer cette puissance. *Annales Scientifiques de l’École Normale Supérieure* **1**, 393–457 (1872). <https://doi.org/10.24033/asens.88>
- [6] T. Li, S. Kheifets, D. Medellin, M.G. Raizen, Measurement of the Instantaneous Velocity of a Brownian Particle. *Science* **328**(5986), 1673–1675 (2010). <https://doi.org/10.1126/science.1189403>
- [7] V. Bickle, C. Bechinger, Realization of a micrometre-sized stochastic heat engine. *Nat. Phys.* **8**(2), 143–146 (2012). <https://doi.org/10.1038/nphys2163>
- [8] P.A. Quinto-Su, A microscopic steam engine implemented in an optical tweezer. *Nat. Commun.* **5**(1), 5889 (2014). <https://doi.org/10.1038/ncomms6889>
- [9] I.A. Martínez, É. Roldán, L. Dinis, D. Petrov, J.M.R. Parrondo, R.A. Rica, Brownian Carnot engine. *Nat. Phys.* **12**(1), 67–70 (2016). <https://doi.org/10.1038/nphys3518>
- [10] Y.H. Chen, J.F. Chen, Z. Fei, H.T. Quan, Microscopic theory of the Curzon-Ahlborn heat engine based on a Brownian particle. *Phys. Rev. E* **106**(2), 024105 (2022). <https://doi.org/10.1103/PhysRevE.106.024105>
- [11] P. Salamon, R.S. Berry, Thermodynamic Length and Dissipated Availability. *Phys.*

Rev. Lett. **51**(13), 1127–1130 (1983). <https://doi.org/10.1103/PhysRevLett.51.1127>

[12] K. Sekimoto, S. ichi Sasa, Complementarity relation for irreversible process derived from stochastic energetics. J. Phys. Soc. Jpn. **66**, 3326–3328 (1997). <https://doi.org/10.1143/JPSJ.66.3326>

[13] A. Bérut, A. Arakelyan, A. Petrosyan, S. Ciliberto, R. Dillenschneider, E. Lutz, Experimental verification of Landauer’s principle linking information and thermodynamics. Nature **483**(7388), 187–189 (2012). <https://doi.org/10.1038/nature10872>

[14] Y.H. Ma, D. Xu, H. Dong, C.P. Sun, Universal constraint for efficiency and power of a low-dissipation heat engine. Phys. Rev. E **98**(4), 042112 (2018). <https://doi.org/10.1103/PhysRevE.98.042112>

[15] Y.H. Ma, R.X. Zhai, J. Chen, C.P. Sun, H. Dong, Experimental Test of the $1/\tau$ -Scaling Entropy Generation in Finite-Time Thermodynamics. Phys. Rev. Lett. **125**(21), 210601 (2020). <https://doi.org/10.1103/PhysRevLett.125.210601>

[16] T. Van Vu, Y. Hasegawa, Geometrical Bounds of the Irreversibility in Markovian Systems. Phys. Rev. Lett. **126**(1), 010601 (2021). <https://doi.org/10.1103/PhysRevLett.126.010601>

[17] M. Esposito, K. Lindenberg, C. Van Den Broeck, Universality of Efficiency at Maximum Power. Phys. Rev. Lett. **102**(13), 130602 (2009). <https://doi.org/10.1103/PhysRevLett.102.130602>

[18] M. Esposito, R. Kawai, K. Lindenberg, C. Van Den Broeck, Efficiency at Maximum Power of Low-Dissipation Carnot Engines. Phys. Rev. Lett. **105**(15), 150603 (2010). <https://doi.org/10.1103/PhysRevLett.105.150603>

[19] S. Deffner, Kibble-Zurek scaling of the irreversible entropy production. Phys. Rev. E **96**(5), 052125 (2017). <https://doi.org/10.1103/PhysRevE.96.052125>

[20] J. Deng, Q.h. Wang, Z. Liu, P. Hänggi, J. Gong, Boosting work characteristics and overall heat-engine performance via shortcuts to adiabaticity: Quantum and classical systems. Phys. Rev. E **88**(6), 062122 (2013). <https://doi.org/10.1103/PhysRevE.88.062122>

[21] D. Guéry-Odelin, A. Ruschhaupt, A. Kiely, E. Torrontegui, S. Martínez-Garaot, J.G. Muga, Shortcuts to adiabaticity: Concepts, methods, and applications. Rev. Mod. Phys. **91**(4), 045001 (2019). <https://doi.org/10.1103/RevModPhys.91.045001>

[22] J.P. Pekola, B. Karimi, G. Thomas, D.V. Averin, Supremacy of incoherent sudden cycles. Phys. Rev. B **100**(8), 085405 (2019). <https://doi.org/10.1103/PhysRevB.100.085405>

[23] P.W. Claeys, M. Pandey, D. Sels, A. Polkovnikov, Floquet-Engineering Counterdiabatic Protocols in Quantum Many-Body Systems. Phys. Rev. Lett. **123**(9), 090602 (2019). <https://doi.org/10.1103/PhysRevLett.123.090602>

[24] T. Villazon, A. Polkovnikov, A. Chandran, Swift heat transfer by fast-forward driving in open quantum systems. Phys. Rev. A **100**(1), 012126 (2019). <https://doi.org/10.1103/PhysRevA.100.012126>

[25] V. Cavina, P.A. Erdman, P. Abiuso, L. Tolomeo, V. Giovannetti, Maximum-power heat engines and refrigerators in the fast-driving regime. Phys. Rev. A **104**(3), 032226 (2021). <https://doi.org/10.1103/PhysRevA.104.032226>

[26] Y.H. Ma, C.P. Sun, H. Dong, Consistency of optimizing finite-time Carnot engines with the low-dissipation model in the two-level atomic heat engine. Commun. Theor. Phys. **73**(12), 125101 (2021). <https://doi.org/10.1088/1572-9494/ac2cb8>

[27] T. Schmiedl, U. Seifert, Efficiency at maximum power: An analytically solvable model for stochastic heat engines. Europhys Lett. **81**(2), 20003 (2008). <https://doi.org/10.1209/0295-5075-81-20003>

[28] D.S.P. Salazar, S.A. Lira, Stochastic thermodynamics of nonharmonic oscillators in high vacuum. *Phys. Rev. E* **99**(6), 062119 (2019). <https://doi.org/10.1103/PhysRevE.99.062119>

[29] S. Krishnamurthy, R. Ganapathy, A.K. Sood, Overcoming power-efficiency trade-off in a micro heat engine by engineered system-bath interactions. *Nat. Commun.* **14**(1), 6842 (2023). <https://doi.org/10.1038/s41467-023-42350-y>

[30] E.B. Richman, N. Ticea, W.E. Allen, K. Deisseroth, L. Luo, Neural landscape diffusion resolves conflicts between needs across time. *Nature* **623**(7987), 571–579 (2023). <https://doi.org/10.1038/s41586-023-06715-z>

[31] S. Kato, F.G. Rose, Global and Regional Entropy Production by Radiation Estimated from Satellite Observations. *Journal of Climate* **33**(8), 2985–3000 (2020). <https://doi.org/10.1175/JCLI-D-19-0596.1>

[32] M. Brunelli, L. Fusco, R. Landig, W. Wieczorek, J. Hoelscher-Obermaier, G. Landi, F.L. Semião, A. Ferraro, N. Kiesel, T. Donner, G. De Chiara, M. Paternostro, Experimental Determination of Irreversible Entropy Production in out-of-Equilibrium Mesoscopic Quantum Systems. *Phys. Rev. Lett.* **121**(16), 160604 (2018). <https://doi.org/10.1103/PhysRevLett.121.160604>

[33] G.T. Landi, M. Paternostro, Irreversible entropy production: From classical to quantum. *Rev. Mod. Phys.* **93**(3), 035008 (2021). <https://doi.org/10.1103/RevModPhys.93.035008>

[34] E. Roduner, T.P. Krüger, The origin of irreversibility and thermalization in thermodynamic processes. *Phys. Rep.* **944**, 1–43 (2022). <https://doi.org/10.1016/j.physrep.2021.11.002>

[35] M.H. Rubin, Optimal configuration of a class of irreversible heat engines. I. *Phys. Rev. A* **19**(3), 1272–1276 (1979). <https://doi.org/10.1103/PhysRevA.19.1272>

[36] P. Salamon, A. Nitzan, B. Andresen, R.S. Berry, Minimum entropy production and the optimization of heat engines. *Phys. Rev. A* **21**(6), 2115–2129 (1980). <https://doi.org/10.1103/PhysRevA.21.2115>

[37] D.S. Seara, B.B. Machta, M.P. Murrell, Irreversibility in dynamical phases and transitions. *Nat. Commun.* **12**(1), 392 (2021). <https://doi.org/10.1038/s41467-020-20281-2>

[38] C. Jarzynski, Equalities and Inequalities: Irreversibility and the Second Law of Thermodynamics at the Nanoscale. *Annu. Rev. Condens. Matter Phys.* **2**(1), 329–351 (2011). <https://doi.org/10.1146/annurev-conmatphys-062910-140506>

[39] U. Seifert, Stochastic thermodynamics, fluctuation theorems and molecular machines. *Rep. Prog. Phys.* **75**(12), 126001 (2012). <https://doi.org/10.1088/0034-4885/75/12/126001>

[40] V. Cavina, A. Mari, V. Giovannetti, Slow Dynamics and Thermodynamics of Open Quantum Systems. *Phys. Rev. Lett.* **119**(5), 050601 (2017). <https://doi.org/10.1103/PhysRevLett.119.050601>

[41] Y.H. Ma, D. Xu, H. Dong, C.P. Sun, Optimal operating protocol to achieve efficiency at maximum power of heat engines. *Phys. Rev. E* **98**(2), 022133 (2018). <https://doi.org/10.1103/PhysRevE.98.022133>

[42] K. Proesmans, J. Ehrich, J. Bechhoefer, Finite-Time Landauer Principle. *Phys. Rev. Lett.* **125**(10), 100602 (2020). <https://doi.org/10.1103/PhysRevLett.125.100602>

[43] X.H. Zhao, Z.C. Tu, Y.H. Ma, Engineering ratchet-based particle separation via extended shortcuts to isothermality. *Phys. Rev. E* **110**(3), 034105 (2024). <https://doi.org/10.1103/PhysRevE.110.034105>

[44] D. Wang, D. Xu, Nonadiabatic evolution and thermodynamics of a time-dependent open quantum system. *Phys. Rev. A* **104**(3),

032201 (2021). <https://doi.org/10.1103/PhysRevA.104.032201>

- [45] Y.H. Ma, Simple realization of the polytropic process with a finite-sized reservoir. *Am. J. Phys.* **91**(7), 555 (2023). <https://doi.org/10.1119/5.0104382>
- [46] D. Dai, Z. Liu, R. Long, F. Yuan, W. Liu, An irreversible Stirling cycle with temperature difference both in non-isothermal and isochoric processes. *Energy* **186**, 115875 (2019). <https://doi.org/10.1016/j.energy.2019.115875>
- [47] Y. Wang, E. Lei, Y.H. Ma, Z.C. Tu, G. Li, Thermodynamic geometric control of active matter. *Phys. Rev. E* **112**, 054124 (2025). <https://doi.org/10.1103/p2gz-47vt>

Supplemental Materials

This document is devoted to providing the detailed derivations and for supporting discussions to the main text. The contents of the Supplemental Materials are listed as follows

Contents

1	The detailed derivation for polytropic steering of underdamped Brownian particles	2
1.1	The effective temperature evolution and polytropic protocols	2
1.2	Thermodynamic quantities and the irreversible entropy generation	2
2	The stochastic framework for polytropic steering of overdamped Brownian particles	3
2.1	Langevin dynamics	3
2.2	The effective temperature evolution and polytropic protocols	3
2.3	Thermodynamic quantities and the irreversible entropy generation	4
3	The asymptotic scaling analysis of irreversible entropy generation	4
3.1	The adiabatic limit	5
3.2	The isothermal limit	5
4	The role of the initial temperature offset δ	5
5	Simulation details	6
5.1	The numerical Solution of the Control Protocol	6
5.2	Langevin Dynamics Simulation	7
5.3	The calculation of thermodynamic quantities	7
5.4	The convergence and Robustness Verification	7
6	The polytropic steering of the ideal gas system	7
6.1	The finite-time polytropic process	8
6.2	The qualification of irreversibility	9
6.3	The application in thermodynamic cycles	9

1 The detailed derivation for polytropic steering of underdamped Brownian particles

In this section, we provide detailed derivation for the polytropic steering of a Brownian particle in the underdamped limit discussed in the main text.

1.1 The effective temperature evolution and polytropic protocols

By leveraging the Fokker–Planck equation corresponding to the Eq. (2) from the main text, we can derive a Maxwell–Boltzmann distribution. Through this distribution correspondence, a rigorous definition of the effective temperature $\theta(t) = 2 \langle E(t) \rangle / f_n$ can be established. Subsequently, based on the first law of thermodynamics, the time-dependent evolution function for the particle’s effective temperature can be deduced as

$$\dot{\theta}(t) = \frac{\dot{\lambda}(t)}{\lambda(t)} \theta(t) - \Gamma_n [\theta(t) - T_s]. \quad (\text{S1})$$

We now impose the polytropic constraint, defined by the relation $\theta \lambda^\xi = \text{const.}$, where ξ is the polytropic index and const. is a constant determined by the initial conditions (k_0, θ_0) . Time differentiation of this constraint yields $\dot{\lambda}/\lambda = -\dot{\theta}/(\xi \theta)$. Substituting this relation into the dynamical equation (S1), we obtain

$$\dot{\theta}(t) = -\frac{\dot{\theta}(t)}{\xi} - \Gamma_n [\theta(t) - T_s]. \quad (\text{S2})$$

With the initial condition $\theta|_{t=0} \equiv \theta_0 = (1 + \delta) T_s$ ($\delta \neq 0$, $\delta < 0$ for expansion, $\delta > 0$ for compression), the above differential equation (S2) is solved as

$$\theta = \theta(t) = \delta T_s \exp\left(-\frac{\xi \Gamma_n}{\xi + 1} t\right) + T_s, \quad (\text{S3})$$

and correspondingly, the work parameter change during the polytropic process $\theta(t) \lambda^\xi(t) = \theta_0 \lambda_0^\xi$ follows as

$$\lambda(t) = \lambda_0 \left[\frac{\delta}{1 + \delta} \exp\left(-\frac{\xi \Gamma_n}{\xi + 1} t\right) + \frac{1}{1 + \delta} \right]^{-\frac{1}{\xi}} \quad (\text{S4})$$

with λ_0 is the initial work parameter of the particle. For the case where $\lambda_f / \lambda_0 \equiv u$ ($\lambda_f = \lambda(\tau)$) is given, where u is the compression ratio of the process, the relation between the normalized process duration $\tilde{\tau} \equiv \tau / \tau_r$ and the polytropic index can be derived from Eq. (S4) as

$$\tilde{\tau} = -\frac{1 + \xi}{\xi} \ln \left[\frac{(1 + \delta) u^{-\xi} - 1}{\delta} \right]. \quad (\text{S5})$$

Eqs. (S4) and (S5) serve as practical operational protocols to realize the given ξ polytropic process.

1.2 Thermodynamic quantities and the irreversible entropy generation

The ensemble average of internal energy for the underdamped Brownian particle can be expressed as $\langle E \rangle = f_n \theta(t)/2$. The increment of trajectory ensemble average work for this system is

$$\langle dW \rangle = \frac{f_n}{2} \theta_0 \lambda_0^\xi \lambda^{-\xi-1} d\lambda. \quad (\text{S6})$$

Integrate from initial (k_0, θ_0) to final (k_f, θ_f) states, we have

$$W = \frac{f_n (1 + \delta) T_s}{2 \xi} [1 - u^{-\xi}]. \quad (\text{S7})$$

Using the first law of thermodynamics we have the heat as

$$Q = \frac{f_n (1 + \delta) T_s}{2} \left(\frac{\xi + 1}{\xi} \right) [u^{-\xi} - 1]. \quad (\text{S8})$$

Finally, we evaluate the irreversible entropy generation (IEG), which in this regime arises from the heat flux between the system at effective temperature θ and the reservoir at T_s . The corresponding IEG rate reads $\dot{S}_{\text{ir}} = \dot{Q}/\theta - \dot{Q}/T_s$. Utilizing the energy balance $\dot{Q} = \dot{E} - \dot{W}$, the cumulative IEG over a duration τ is given by

$$\Delta S_{\text{ir}} = \int_0^\tau \left(\frac{\dot{E} - \dot{W}}{\theta} - \frac{\dot{E} - \dot{W}}{T_s} \right) dt. \quad (\text{S9})$$

By substituting the polytropic trajectories and the control equation (S4), the analytical expression for IEG is simplified to

$$\Delta S_{\text{ir}} = (\xi + 1) [\xi^{-1}(1 + \delta)(1 - u^{-\xi}) - \ln u], \quad (\text{S10})$$

where $u = k_f/k_0$ is the compression/expansion ratio. This result recovers the universal scaling behavior discussed in the main text, confirming that the thermodynamic cost of polytropic steering is preserved in the underdamped regime.

2 The stochastic framework for polytropic steering of overdamped Brownian particles

In this section, we establish a stochastic derivation for the polytropic steering of a Brownian particle in the overdamped limit. This framework provides the theoretical basis for the control protocols and thermodynamic quantities discussed in the main text.

2.1 Langevin dynamics

We consider a one-dimensional overdamped Brownian particle confined within a time-dependent harmonic potential $U(x, k_t) = k_t x^2/2$ for simplicity and without loss of generality. The governing Langevin equation in the overdamped limit is given by

$$\gamma \dot{x} = -\frac{k_t}{m} x + \frac{\zeta(t)}{m}, \quad (\text{S11})$$

where γ denotes the friction coefficient. To ensure the consistency of the steady-state distribution with the Boltzmann factor $P_{\text{eq}}(x) \propto e^{-U/T_s}$, the stochastic force $\zeta(t)$ must satisfy the fluctuation-dissipation theorem

$$\langle \zeta(t) \zeta(t') \rangle = 2m\gamma T_s \delta(t - t'), \quad (\text{S12})$$

where T_s is the temperature of the heat reservoir. By representing the white noise as a Wiener increment, $\xi(t) dt = \sqrt{2m\gamma T_s} dW_t$, Eq. (S11) can be recast into the Ito stochastic differential equation

$$dx = -\frac{k_t}{m\gamma} x dt + \sqrt{\frac{2T_s}{m\gamma}} dW_t. \quad (\text{S13})$$

To track the energetic evolution of the system, we define the instantaneous energy as $E(t) = U(x(t), t) = \frac{1}{2} k_t x(t)^2$. According to Ito's lemma, the differential of a scalar function $f(x, t)$ is expressed as

$$df = \partial_t f dt + \partial_x f dx + \frac{1}{2} \partial_{xx} f (dx)^2. \quad (\text{S14})$$

By substituting the specific form of the harmonic potential into Eq. (S14) and utilizing the property $(dW_t)^2 = dt$, the stochastic increment of the system energy is derived as

$$dE = \left(\frac{1}{2} \dot{k}_t x^2 - \frac{k_t^2}{m\gamma} x^2 + \frac{k_t T_s}{m\gamma} \right) dt + k_t x \sqrt{\frac{2T_s}{m\gamma}} dW_t. \quad (\text{S15})$$

2.2 The effective temperature evolution and polytropic protocols

Following the framework of stochastic thermodynamics, the ensemble-averaged energy $\langle E \rangle$ can be associated with an effective temperature $\theta(t)$ via the relation $\langle E \rangle = \frac{1}{2} \theta(t)$ [1]. Taking the expectation of Eq. (S15) and noting that the expectation of the Wiener term vanishes, we obtain the dynamical equation for $\theta(t)$

$$\dot{\theta} = \frac{\dot{k}_t}{k_t} \theta - \frac{2k_t}{m\gamma} (\theta - T_s). \quad (\text{S16})$$

Equation (S16) describes the thermal relaxation of the particle towards the reservoir temperature T_s , modulated by the active variation of the trap stiffness k_t .

We now impose the polytropic constraint, defined by the relation $\theta k_t^\xi = \text{const.}$, where ξ is the polytropic index and const. is a constant determined by the initial conditions (k_0, θ_0) . Time differentiation of this constraint yields $\dot{k}_t/k_t = -\dot{\theta}/(\xi\theta)$. Substituting this relation into the dynamical equation (S16) yields the steering protocol for the trap stiffness

$$\frac{\dot{k}_t}{k_t} = \frac{2k_t}{m\gamma(\xi+1)} \left[1 - \frac{1}{1+\delta} \left(\frac{k_t}{k_0} \right)^\xi \right], \quad (\text{S17})$$

where $\delta = (\theta_0 - T_s)/T_s$ characterizes the initial thermal deviation from the reservoir.

2.3 Thermodynamic quantities and the irreversible entropy generation

The average work rate is defined by the variation of the potential parameters, $\langle \dot{W} \rangle = \frac{1}{2} \langle x^2 \rangle \dot{k}_t$. With the relation $\langle x^2 \rangle = \theta/k_t$, the total work performed during a process from k_0 to k_f is integrated as

$$W = \frac{\theta_0}{2\xi} \left[1 - \left(\frac{k_0}{k_f} \right)^\xi \right] \quad (\text{S18})$$

Applying the first law of thermodynamics, $\Delta E = W + Q$, where $\Delta E = (\theta_f - \theta_0)/2$, the heat exchanged with the reservoir is obtained as

$$Q = \frac{\theta_0}{2} \left(\frac{\xi+1}{\xi} \right) \left[\left(\frac{k_0}{k_f} \right)^\xi - 1 \right]. \quad (\text{S19})$$

Finally, we evaluate the irreversible entropy generation (IEG), which in this regime arises from the heat flux between the system at effective temperature θ and the reservoir at T_s . The corresponding IEG rate reads $\dot{S}_{\text{ir}} = \dot{Q}/\theta - \dot{Q}/T_s$ [2]. Utilizing the energy balance $\dot{Q} = \dot{E} - \dot{W}$, the cumulative IEG over a duration τ is given by

$$\Delta S_{\text{ir}} = \int_0^\tau \left(\frac{\dot{E} - \dot{W}}{\theta} - \frac{\dot{E} - \dot{W}}{T_s} \right) dt. \quad (\text{S20})$$

By substituting the polytropic trajectories and the control equation (S17), the analytical expression for IEG is simplified to

$$\Delta S_{\text{ir}} = \frac{1}{2} (\xi+1) [\xi^{-1} (1+\delta) (1 - u^{-\xi}) - \ln u], \quad (\text{S21})$$

where $u = k_f/k_0$ is the compression/expansion ratio. This result recovers the universal scaling behavior discussed in the main text, confirming that the thermodynamic cost of polytropic steering is preserved in the overdamped regime.

3 The asymptotic scaling analysis of irreversible entropy generation

As discussed in the main text, the irreversible entropy generation (IEG) exhibits a non-monotonic dependence on the process duration $\tilde{\tau}$, characterized by a transition from linear growth in the fast-driving regime to a $1/\tilde{\tau}$ decay in the quasi-static limit. To rigorously elucidate the mathematical origin of these scaling laws, this section provides an asymptotic analysis of the IEG near the two fundamental thermodynamic boundaries: the adiabatic limit ($\xi \rightarrow -1$) and the isothermal limit ($\xi \rightarrow 0$).

The IEG for a system of underdamped Brownian particles in the Section 1 reads

$$\Delta S_{\text{ir}} = (\xi+1) [\xi^{-1} (1+\delta) (1 - u^{-\xi}) - \ln u], \quad (\text{S22})$$

together with the corresponding the $\tau - \xi$ relation

$$\tilde{\tau} = -(1 + \xi^{-1}) \ln [(1 + \delta^{-1}) u^{-\xi} - \delta^{-1}]. \quad (\text{S23})$$

Taylor expansions of Eqs. (S22) and (S23) around $\xi = 0$ and $\xi = -1$ yield the analytical coefficients that govern dissipation in the adiabatic and isothermal regimes, respectively.

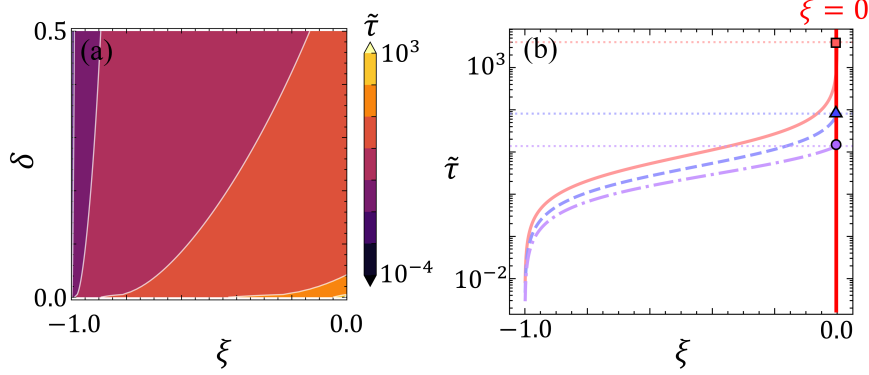


Fig. S1 The influence of initial temperature offset δ on the duration, and $u = 1.5$ is used in this figure. (a) The heatmap of the normalized process duration $\tilde{\tau}$ as functions of ξ and δ . (b) $\tilde{\tau}$ versus ξ for three different $\delta = 10^{-4}$ (pink solid curve), 5×10^{-3} (blue dashed curve), and 3×10^{-2} (purple dash-dotted curve). The maximum process durations $\tilde{\tau}_{\max}$ corresponding to $\xi = 0$ are marked with the pink square, blue triangle, and purple circle.

3.1 The adiabatic limit

For adiabatic regime, $\tilde{\tau}$ can be expressed as

$$\tilde{\tau} \approx A_{-1}(\xi + 1). \quad (\text{S24})$$

Additionally, the Taylor expression of ΔS_{ir} at $\xi = -1$ denotes as

$$\Delta S_{\text{ir}} \approx B_{-1}(\xi + 1). \quad (\text{S25})$$

Finally, we can obtain

$$\Delta S_{\text{ir}} \approx \kappa_1(\delta, u)\tilde{\tau} = \frac{B_{-1}}{A_{-1}}\tau, \quad (\text{S26})$$

where

$$A_{-1} = \ln \left[\frac{(1 + \delta)u - 1}{\delta} \right], \quad B_{-1} = (1 + \delta)(u - 1) - \ln u.$$

3.2 The isothermal limit

For isothermal regime, the expansion approximation of $\tilde{\tau}$ can be expressed as

$$\frac{1}{\tilde{\tau}} \approx A_0 + B_0\xi. \quad (\text{S27})$$

Additionally, we can obtain

$$\Delta S_{\text{ir}} \approx C_0 + D_0\xi. \quad (\text{S28})$$

Finally, we have

$$\Delta \tilde{S}_{\text{ir}} \approx \kappa_2(\delta, u)/\tilde{\tau} + \kappa_0(\delta, u) = \frac{D_0}{B_0} \frac{1}{\tilde{\tau}} + C_0 - \frac{A_0 D_0}{B_0}, \quad (\text{S29})$$

where

$$A_0 = \frac{\delta}{(1 + \delta) \ln u}, \quad B_0 = -\frac{\ln u + 2\delta}{2(1 + \delta) \ln u}, \quad C_0 = \delta \ln u, \quad D_0 = \delta \ln u - \frac{1}{2}(1 + \delta) \ln^2 u.$$

4 The role of the initial temperature offset δ

As noted in the main text, the realization of a finite-time polytropic process is contingent upon a non-zero initial temperature offset $\delta \equiv \theta_0/T_s - 1$. This section demonstrates the mathematical necessity of this non-equilibrium starting point and examines how the δ dictate $\tilde{\tau}$ and IEG.

The governing equation for the finite-time polytropic process reveals a mathematical singularity when $\delta = 0$. Physically, this implies that if a system begins in perfect equilibrium with the reservoir, a quasi-static polytropic path with a specific index ξ (other than the isothermal or isochoric limits) cannot be uniquely initiated without an infinitesimal heat flow to select the trajectory. However, we demonstrate that the limit $\delta \rightarrow 0$ is well-behaved, as shown in Figs. S1 and S2. For any arbitrarily small but finite perturbation, the

control protocol remains robust and experimentally accessible (very rapid quenching from the equilibrium state).

As illustrated in Fig. S1, the limit $\xi = 0$ corresponds to an endoreversible isothermal process. For a given initial temperature offset δ , the process duration is characterized by a finite timescale that diverges only as $\delta \rightarrow 0$, thereby recovering the conventional quasi-static limit. This behavior is further corroborated by the entropy analysis in Fig. S2, which reveals that a perfectly reversible isothermal transformation is attainable only in the limit of vanishing δ . The existence of an initial temperature gradient inherently induces an irreversible entropy flux and the asymptotic points provided in the isothermal limit confirm this dissipation mechanism arising from initial thermal mismatch.

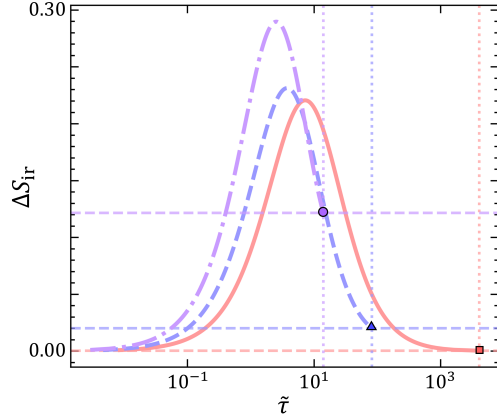


Fig. S2 ΔS_{ir} versus $\tilde{\tau}$ for three different $\delta = 10^{-4}$ (pink solid curve), 5×10^{-3} (blue dashed curve), and 3×10^{-2} (purple dash-dotted curve). The theoretical isothermal limits are given by dotted line. The maximum process durations $\tilde{\tau}_{\text{max}}$ corresponding to $\xi = 0$ are marked with the pink square, blue triangle, and purple circle.

5 Simulation details

In this section, we provide an in-depth description on how all our numerical simulations are implemented. To validate the theoretical predictions of the polytropic process for an overdamped Brownian particle, we performed numerical simulations of the stochastic Langevin dynamics. The simulation framework consists of three coupled parts: (i) the numerical solution of the control protocol k_t , (ii) the ensemble simulation of particle trajectories, and (iii) a rigorous convergence verification.

5.1 The numerical Solution of the Control Protocol

The time evolution of the trap stiffness k_t , required to maintain the polytropic condition $\theta k^\xi = \text{const.}$, is governed by the nonlinear ordinary differential equation (ODE) derived in the main text,

$$\frac{\dot{k}_t}{k_t} = \frac{2k_t}{m\gamma(\xi+1)} \left[1 - \frac{1}{1+\delta} \left(\frac{k_t}{k_0} \right)^\xi \right]. \quad (\text{S30})$$

We solved this initial value problem using the `scipy.integrate.solve_ivp` package in Python.

Algorithm Selection: To ensure numerical stability particularly when the polytropic index ξ approaches the singular value of -1 , we implemented an adaptive solver strategy:

- For general cases, we utilized the explicit Runge-Kutta method of order 5(4) (RK45).
- For cases where $\xi \approx -1$ (specifically $|\xi+1| < 10^{-2}$), the dynamics become stiff. Here, we switched to the Backward Differentiation Formula (BDF) method.
- To prevent numerical division errors, a regularization parameter $\epsilon = 10^{-12}$ was applied to the denominator term $(\xi+1)$.

Event Detection: The duration of the protocol τ was determined dynamically. We employed a root-finding event detection algorithm to identify the precise time instant $t = \tau$ at which the stiffness reached the target compression value $k(\tau) = k_{\text{final}}$.

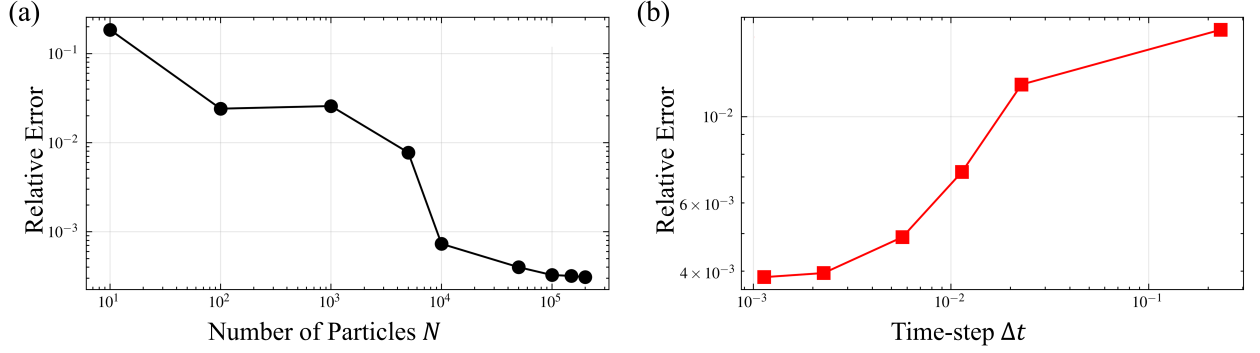


Fig. S3 Relative Error of work as a function of (a) ensemble size N and (b) time-step Δt .

5.2 Langevin Dynamics Simulation

Discretization Scheme: We simulated the trajectories of an ensemble of $N = 10^6$ non-interacting particles using the Euler-Maruyama scheme. The iterative update rule for the position x_n of the n -th particle at time step j is given by

$$x_n(t_{j+1}) = x_n(t_j) - \frac{k(t_j)}{\gamma} x_n(t_j) \Delta t + \sqrt{\frac{2T_s \Delta t}{\gamma}} \mathcal{N}(0, 1), \quad (\text{S31})$$

where Δt is the time step. The initial positions $\{x_n(0)\}$ were sampled from the equilibrium Boltzmann distribution $P(x, 0) \propto \exp(-U/\theta_0)$.

5.3 The calculation of thermodynamic quantities

Thermodynamic observables were computed via ensemble averaging over the N simulated trajectories.

- Effective Temperature: $\theta_{\text{sim}} = k(t) \langle x^2(t) \rangle \approx \frac{k(t)}{N} \sum_{n=1}^N x_n^2(t)$.
- Stochastic Work: To ensure numerical accuracy, we employed the midpoint approximation for the position term in the discretized work $dW = \frac{1}{2}x^2 dk$ as

$$W(t) = \sum_{j=0}^{M(t)} \frac{1}{2} \left[\frac{x_n^2(t_j) + x_n^2(t_{j+1})}{2} \right] (k(t_{j+1}) - k(t_j)), \quad (\text{S32})$$

where $M(t)$ denote the time discretization of total steps.

- Heat Q was derived using $Q(t) = \Delta U(t) - W(t)$, where $\Delta U(t) = \frac{1}{2}k(t)x^2(t) - \frac{1}{2}k_0x^2(0)$.

5.4 The convergence and Robustness Verification

To ensure the reliability of the numerical results, we conducted comprehensive convergence tests

- Ensemble Size Convergence (N): increasing N from 10^1 to 10^5 reduces the relative error compared to the analytical solution to below 0.1%.
- Time-step Convergence (Δt): The discretization error of the Euler-Maruyama scheme was monitored by varying Δt . We ensured that Δt is significantly smaller than the instantaneous relaxation time $\tau_r = \gamma/k(t)$ throughout the protocol. A convergence of the error with respect to Δt was observed.

6 The polytropic steering of the ideal gas system

In the main text, we established a finite-time polytropic steering framework for Brownian particles, focusing on the interplay between stochastic energetics and time-dependent confinement. To demonstrate the broader universality of this paradigm, we now extend the polytropic steering principle to a macroscopic classical system—the ideal gas. The objective of this section is to show that the protocols derived for microscopic stochastic systems are not mere artifacts of the harmonic potential or specific noise realizations. Instead,

they represent a fundamental class of thermodynamic transformations that can be generalized to any system where the evolution of internal energy follows a consistent linear structure.

6.1 The finite-time polytropic process

The concept of a polytropic process $pV^\xi = \text{const.}$, where p and V denote the pressure and the volume, is a cornerstone of textbook equilibrium thermodynamics, typically introduced as a heuristic interpolation between the idealized isothermal and adiabatic limits. However, in its conventional form, the polytropic paradigm remains a purely phenomenological description of state-space trajectories, lacking a macroscopic kinetic foundation for operations performed in finite time. To bridge this gap, we consider a dynamic model of an ideal gas where the finite-time heat exchange with the environment is explicitly accounted for.

The system is thermally isolated from the external environment and comprises an ideal gas with temperature T driven by a heat reservoir with constant temperature T_s . When the gas is compressed or expanded by a piston, the energy conservation ($\dot{U} = \dot{Q} + \dot{W}$) law reads

$$C_V \dot{T} = -\kappa(T - T_s) - p \dot{V}. \quad (\text{S33})$$

Here, C_V represents the heat capacity of an ideal gas at constant volume, and the heat transfer is assumed to follow Newton's law of cooling with the coefficient κ . Note that $\tau_r = C_V/\kappa$ is the characteristic time for the gas to thermalize in the reservoir, which is much larger than the internal relaxation time t_{in} of the gas [2]. The polytropic process equation can be written in terms of T and V as $TV^{\xi-1} = \text{constant}$, differentiating which with respect to time yields

$$\dot{T}V + (\xi - 1)T\dot{V} = 0. \quad (\text{S34})$$

From Eq. (S33), eliminating p with the ideal gas state equation $pV = NT$ and further eliminating V and \dot{V} with Eq. (S34), we obtain

$$C_V \dot{T} = -\kappa(T - T_s) + N \frac{\dot{T}}{\xi - 1}, \quad (\text{S35})$$

where N is the gas particle number. With the initial condition $T|_{t=0} \equiv T_0 = (1 + \delta)T_e$ ($\delta \neq 0$, $\delta < 0$ for expansion, and $\delta > 0$ for compression), the above differential equation is solved as

$$T = T(t) = \delta T_s \exp \left[\frac{\kappa(\gamma - 1)(\xi - 1)}{N(\gamma - \xi)} t \right] + T_s, \quad (\text{S36})$$

and correspondingly, the volume change during the polytropic process $T(t)[V(t)]^{(\xi-1)} = T_0 V_0^{(\xi-1)}$ follows as

$$V(t) = V_0 \left\{ \frac{\delta}{1 + \delta} \exp \left[\frac{\kappa(\gamma - 1)(\xi - 1)}{N(\gamma - \xi)} t \right] + \frac{1}{1 + \delta} \right\}^{\frac{1}{1 - \xi}}, \quad (\text{S37})$$

where V_0 is the initial volume of the gas.

For the case where $V_f/V_0 \equiv u$ ($V_f = V(\tau)$) is given, where u is the compression ratio of the process, the relation between the normalized process duration $\tilde{\tau} \equiv \tau/\tau_r$ and the polytropic index can be derived from Eq. (S37) as

$$\tilde{\tau} = \frac{\gamma - \xi}{\xi - 1} \ln \left[\frac{(1 + \delta) u^{1 - \xi} - 1}{\delta} \right]. \quad (\text{S38})$$

Eqs. (S37) and (S38) serve as practical operation protocols to realize the given ξ polytropic process.

It is highly instructive to note that the resulting protocols for the ideal gas [Eqs. (S37)-(S38)] are formally identical to those derived for the underdamped Brownian particle in the main text. This mathematical isomorphism is not coincidental but stems from the fact that both systems, despite their vastly different scales and noise characteristics, share a common governing structure for their temperature (or average energy) evolution. Consequently, the polytropic paradigm can be naturally translated from the stochastic realm to classical engineering systems via a simple mapping of physical parameters—such as substituting the trap stiffness control with piston volume modulation. This unity reinforces the role of the polytropic index as a universal control knob for finite-time thermodynamics.

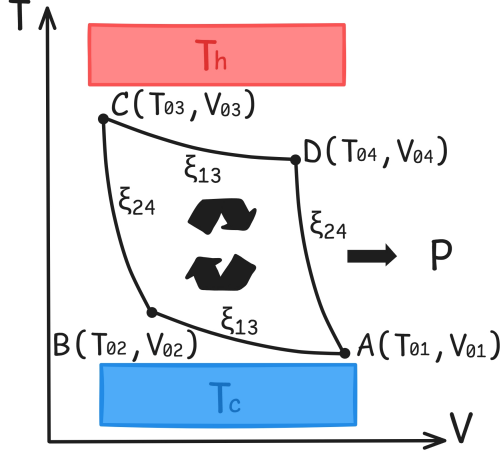


Fig. S4 The schematic T-V diagram of a four strokes polytropic cycle. The processes C→B (polytropic index ξ_{24}) and B→A (ξ_{13}) release heat to the low-temperature reservoir at T_c , while A→D (ξ_{24}) and D→C (ξ_{13}) absorb heat from the high-temperature reservoir at T_h . The cycle outputs net work.

6.2 The qualification of irreversibility

For the ideal gas undergoing the polytropic process of interest, IEG is only attributed to the heat flow resulting from the discrepancy of temperature between the system and the heat reservoir [3], namely, $\Delta S_{\text{ir}} = \int_0^\tau (\dot{Q}/T - \dot{Q}/T_e) dt$, which is specifically obtained as

$$\Delta \tilde{S}_{\text{ir}} = \frac{\gamma - \xi}{\gamma - 1} \left(1 + \frac{\delta + 1}{\xi - 1} \frac{u^{1-\xi} - 1}{\ln u} \right). \quad (\text{S39})$$

Here, we have used $\dot{Q} = C_\xi \dot{T}$ with the polytropic heat capacity $C_\xi = C_V (\xi - \gamma) (\xi - 1)$, $\Delta \tilde{S}_{\text{ir}} \equiv \Delta S_{\text{ir}} / \Delta S_{\text{iso}}$, and $\Delta S_{\text{iso}} = N \ln u$ denotes the reversible entropy change in a quasi-static isothermal process of $\xi = 1$. Substituting Eq. (S38) into the above equation, IEG as a function of process duration is straightforwardly determined.

6.3 The application in thermodynamic cycles

We present a general polytropic cycle of heat engines, as shown in Fig. S4. The closed conditions of the cycle are

$$\begin{aligned} T_{01} V_{01}^{\xi_{13}-1} &= T_{02} V_{02}^{\xi_{13}-1}, \\ T_{02} V_{02}^{\xi_{24}-1} &= T_{03} V_{03}^{\xi_{24}-1}, \\ T_{03} V_{03}^{\xi_{13}-1} &= T_{04} V_{04}^{\xi_{13}-1}, \\ T_{04} V_{04}^{\xi_{24}-1} &= T_{01} V_{01}^{\xi_{24}-1}. \end{aligned} \quad (\text{S40})$$

Since the heat capacity of a polytropic process depends only on the polytropic index, the heat absorbed or released in each process can be straightforwardly calculated based on the parameters of A, B, C, and D as follows

$$\begin{aligned} Q_{A \rightarrow B} &= C_V \frac{\xi_{13} - \gamma}{\xi_{13} - 1} (T_{02} - T_{01}), \\ Q_{B \rightarrow C} &= C_V \frac{\xi_{24} - \gamma}{\xi_{24} - 1} (T_{03} - T_{02}), \\ Q_{C \rightarrow D} &= C_V \frac{\xi_{13} - \gamma}{\xi_{13} - 1} (T_{04} - T_{03}), \\ Q_{D \rightarrow A} &= C_V \frac{\xi_{24} - \gamma}{\xi_{24} - 1} (T_{01} - T_{04}). \end{aligned} \quad (\text{S41})$$

With Eqs. (S40) and (S41), we can obtain the simplified expressions of efficiency and work output of the cycle as

$$\begin{aligned} W &= Q_{A \rightarrow B} + Q_{B \rightarrow C} + Q_{C \rightarrow D} + Q_{D \rightarrow A} \\ &= C_V [T_{01} (\mu^{\xi_{13}-1} - 1) + T_{03} (\mu^{1-\xi_{13}} - 1)] \left(\frac{\xi_{13} - \gamma}{\xi_{13} - 1} - \frac{\xi_{24} - \gamma}{\xi_{24} - 1} \right). \end{aligned} \quad (\text{S42})$$

Here, using Q_a and Q_r to denote the heat absorbed and released respectively, we have

$$\begin{aligned} Q_a &= \frac{1}{2} \{ [1 + \text{sgn}(Q_{A \rightarrow B})] Q_{A \rightarrow B} + [1 + \text{sgn}(Q_{B \rightarrow C})] Q_{B \rightarrow C} \\ &\quad + [1 + \text{sgn}(Q_{C \rightarrow D})] Q_{C \rightarrow D} + [1 + \text{sgn}(Q_{D \rightarrow A})] Q_{D \rightarrow A} \}, \end{aligned} \quad (\text{S43})$$

where

$$\text{sgn}(x) = \begin{cases} -1, & x \leq 0 \\ 1, & x > 0. \end{cases}$$

For specific situation $Q_a = Q_{C \rightarrow D} + Q_{D \rightarrow A}$, we have

$$\begin{aligned} \eta &= \frac{W}{Q_a} = \frac{W}{Q_{C \rightarrow D} + Q_{D \rightarrow A}} \\ &= \frac{(2 - \mu^{\xi_{13}-1} - \mu^{1-\xi_{13}}) + (1 - T_{01}/T_{03}) (\mu^{\xi_{13}-1} - 1)}{1 - \mu^{1-\xi_{13}} + (1 - T_{01}/T_{03}) \frac{(\xi_{24}-\gamma)(\xi_{13}-1)}{(\gamma-1)(\xi_{13}-\xi_{24})}}, \end{aligned} \quad (\text{S44})$$

where $\mu \equiv V_{01}/V_{02} = V_{04}/V_{03}$.

For some particular polytropic index, this efficiency formula can be degenerated into the familiar form. When $\xi_{13} = 1$, $\xi_{24} = \gamma$, $T_{01} = T_c$ and $T_{03} = T_h$, Eq. (S44) is reduced to

$$\begin{aligned} \eta &= \frac{\eta_C (\mu^{\xi_{13}-1} - 1)}{1 - \mu^{1-\xi_{13}}} \\ &= \frac{\eta_C [e^{(\xi_{13}-1) \ln \mu} - 1]}{1 - e^{(1-\xi_{13}) \ln \mu}} \\ &\approx \frac{\eta_C (\xi_{13} - 1) \ln \mu}{(\xi_{13} - 1) \ln \mu} = \eta_C, \end{aligned} \quad (\text{S45})$$

which is back to the result of the Carnot cycle. When $\xi_{13} = 0$, $\xi_{24} = \gamma$, $T_{01} = T_c$ and $T_{03} = T_h$, Eq. (S44) is reduced to

$$\begin{aligned} \eta &= \frac{(2 - \mu^{-1} - \mu) + \eta_C (\mu^{-1} - 1)}{1 - \mu} \\ &= 1 - \mu^{-1} (1 - \eta_C), \end{aligned} \quad (\text{S46})$$

which is back to the result of the Ranking cycle.

To investigate the specific performance of the cycle, we set the symmetric polytropic index ξ , thereby circumventing the complexity while capturing the basic characteristics arising from fast driving protocol. As illustrated in Fig. S5(a), we propose a thermodynamic cycle, termed the polytropic-adiabatic cycle (PAC), which consists of two symmetric polytropic processes with same ξ and two adiabatic processes. The geometric feature of PAC is solely characterized by ξ . As $\xi \rightarrow 1$, PAC converges to endoreversible Carnot cycle; while when $\xi \rightarrow \gamma$, the polytropic and adiabatic processes degenerate, resulting in the cycle disappearing. Note that the cycle duration is entirely contributed by the polytropic processes according to Eq. (S38), such that the efficiency and power of the cycle are explicitly determined by ξ . The trade-off relation between power and efficiency is obtained by varying ξ , as shown in Fig. S5(b). Each local point on this trade-off is plotted with a certain ξ , the value of which is visualized by the color map.

The power-efficiency trade-off relation of PAC exhibits consistent behavior with the $1/\tau$ -scaling. Namely, as ξ decreases (approaching the blue zone of the gradient curve), the cycle efficiency approaches the Carnot limit but at the cost of zero power output. Notably, the EMP of PAC surpasses the upper bound predicted by the Low-Dissipation (LD) model. While similar behavior has been observed in micro quantum systems,

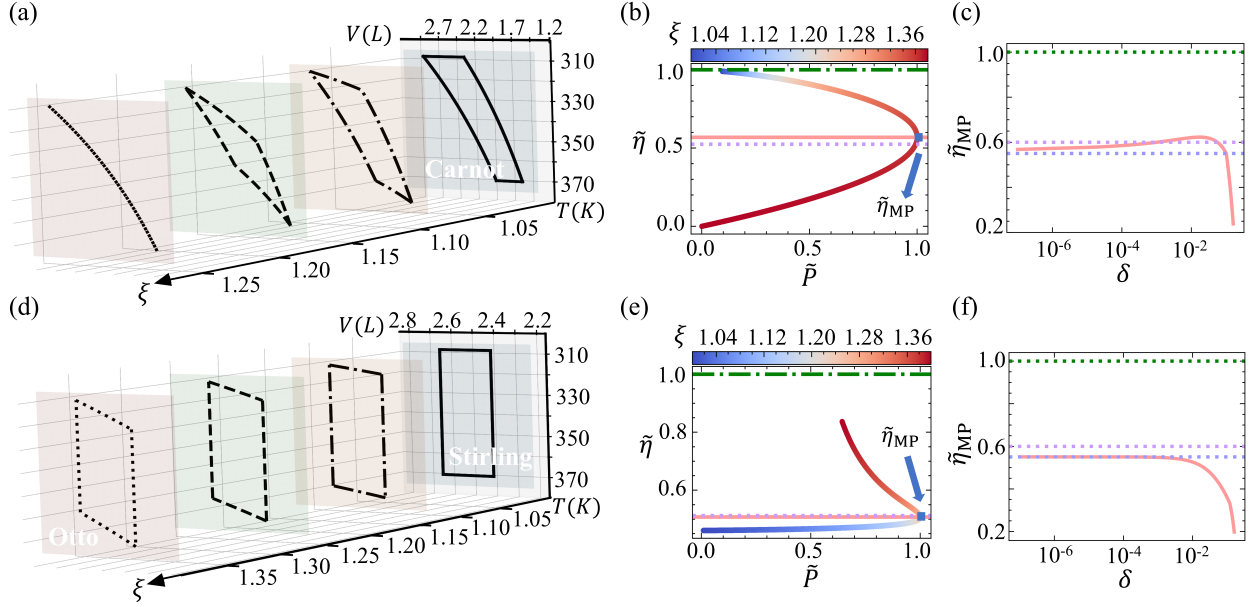


Fig. S5 (a) The transition of the T-V diagram from the endoreversible Carnot cycle to the degenerate of polytropic and adiabatic process with the high- and low-temperature reservoirs set at 369.8 (K) and 308.2 (K), respectively, and a compression ratio of 1.1. (b) Normalized efficiency $\tilde{\eta}$ versus normalized power \tilde{P} trade-off. The dash-dotted green line (upper) shows the Carnot efficiency $\eta_C = 9.1 \times 10^{-2}$, and the EMP of polytropic-adiabatic cycle is highlighted using blue square and pink solid curve. EMP of Low-Dissipation model is given by a purple dotted line. ξ of the cycle is shown with a color map on the trade-off curve. (c) EMP of PAC (solid pink curve) as the function of δ , and the Carnot efficiency, the upper bound of low-dissipation model and CA efficiency are represented as green dotted, purple dotted and blue dotted line, respectively. (d) The transition from the Stirling cycle to the Otto cycle with the high- and low-temperature reservoirs set at 369.8 (K) and 308.2 (K), respectively, and a compression ratio of 1.05. (e) The trade-off between normalized power and normalized efficiency. (f) EMP of polytropic-isochoric (solid curve) as the function of δ , and the Carnot efficiency, the upper bound of LD model and CA efficiency are plotted by green dotted, purple dotted and blue dotted line, respectively.

where phase transitions originate from collective advantages and many-body interactions [4–6], our ideal gas system lacks internal interactions. Consequently, we examine the relation between EMP and δ , as shown in Fig. S5(c). The results indicate that EMP exhibits a nonmonotonic behavior: as δ approaches 0, it converges to the result predicted by the CA model $\eta_{CA} = 1 - \sqrt{1 - \eta_C}$; subsequently, it surpasses the result of the LD model in certain intermediate regions; and finally, it monotonically decreases to 0 as δ further increases.

The Stirling and Otto cycles are practical thermodynamic cycles widely used in engineering applications [7]. By combining polytropic and isochoric processes, we propose a polytropic-isochoric cycle (PIC), which enables a continuous transition from the Stirling cycle ($\xi \rightarrow 1$) to the Otto cycle ($\xi \rightarrow \gamma$) as illustrated in Fig. S5(d). Notably, the time for the isochoric branch must be included in the total cycle time, and both satisfy Eq. (S38). For the isochoric process, this equation corresponds to $\xi \rightarrow \infty$. Increasing ξ has two primary effects: i) it directly reduces the time of the polytropic branch, and ii) it shifts the intersection between the polytropic and isochoric processes upward, thereby reducing the isochoric process time. Overall, the performance of the PIC is solely determined by ξ .

The power-efficiency trade-off relation is depicted in Fig. S5(e), illustrating its behavior during varying ξ . In addition to distinct shapes with PAC, the gradient curves of PIC exhibit reversed colors. Specifically, the power-efficiency trade-off relation of PIC scales with τ : as ξ increases (approaching the red zone of the gradient curve), the cycle efficiency improves correspondingly. This difference arises from the presence of isochoric branches in PIC, which increase IEG compared to the adiabatic branches. The isochoric branches contribute more significantly to the IEG than the polytropic process, owing to their efficient heat exchange and longer thermal relaxation times with the reservoirs. Higher value of ξ can reduce the ratio of isochoric process in PIC, resulting in low dissipation thus higher efficiency. Because of the greater role of the isochoric process in IEG, δ (a key parameter for the polytropic branches) in PIC serves only as an upper bound for the quasi-static cycle efficiency. This differs from its role in PAC, where δ balances power and efficiency at the point of EMP. This distinction also explains why the EMP in PIC varies monotonically with δ , as shown in Fig. S5(f).

References

- [1] Y.H. Chen, J.F. Chen, Z. Fei, H.T. Quan, Microscopic theory of the Curzon-Ahlborn heat engine based on a Brownian particle. *Phys. Rev. E* **106**(2), 024105 (2022). <https://doi.org/10.1103/PhysRevE.106.024105>
- [2] Y.H. Ma, R.X. Zhai, J. Chen, C.P. Sun, H. Dong, Experimental Test of the $1 / \tau$ -Scaling Entropy Generation in Finite-Time Thermodynamics. *Phys. Rev. Lett.* **125**(21), 210601 (2020). <https://doi.org/10.1103/PhysRevLett.125.210601>
- [3] U. Seifert, Stochastic thermodynamics, fluctuation theorems and molecular machines. *Rep. Prog. Phys.* **75**(12), 126001 (2012). <https://doi.org/10.1088/0034-4885/75/12/126001>
- [4] N. Golubeva, A. Imparato, Efficiency at Maximum Power of Interacting Molecular Machines. *Phys. Rev. Lett.* **109**(19), 190602 (2012). <https://doi.org/10.1103/PhysRevLett.109.190602>
- [5] M.L. Bera, S. Julià-Farré, M. Lewenstein, M.N. Bera, Quantum heat engines with Carnot efficiency at maximum power. *Phys. Rev. Res.* **4**(1), 013157 (2022). <https://doi.org/10.1103/PhysRevResearch.4.013157>
- [6] S. Liang, Y.H. Ma, D.M. Busiello, P. De Los Rios, Minimal Model for Carnot Efficiency at Maximum Power. *Phys. Rev. Lett.* **134**(2), 027101 (2025). <https://doi.org/10.1103/PhysRevLett.134.027101>
- [7] D. Dai, Z. Liu, R. Long, F. Yuan, W. Liu, An irreversible Stirling cycle with temperature difference both in non-isothermal and isochoric processes. *Energy* **186**, 115875 (2019). <https://doi.org/10.1016/j.energy.2019.115875>